Parametric study of factors affecting shock-induced flow separation in scramjet intakes

Rachit Singh* and Krishnendu Sinha†
Indian Institute of Technology Bombay, Mumbai, Maharashtra, 400 076, India
†*Corresponding author: krish@aero.iitb.ac.in*

Abstract : High-speed turbulent flow over a scramjet encounters flow-separation due to shock-boundary layer interaction. The variation in separation bubble size with respect to various canonical parameters and the effect of separation bubble on Lift and Drag of the intake for different practical parameters is studied in detail. The scramjet intake is simulated for free-stream conditions corresponding to M_1 = 6 at z =30km and changes in separation bubble size is studied by varying canonical parameters like ramp angle, wall-temperature, Mach number and Reynolds number along with practical parameters like altitude, flight Mach number, ramp length and angle of attack. The well-validated shock-unsteadiness turbulence model is used for the simulations.

Keywords: *Separation bubble, turbulent, boundary layer, wall-temperature, compression corner, Mach number, Reynolds number, Lift, Drag.*

I. Introduction

Air-breathing vehicles such as scramjet are subjected to excessive aerodynamic and thermal load due to generation of shock-waves while cruising at hyper-sonic speeds. The presence of shock-waves becomes more critical if its interaction with the vehicle boundary layer leads to flow-reversal within the boundary layer and formation of separation bubble. Presence of separation bubble can have many adverse effects as it alters of aerodynamic properties of vehicle surface leading to increased drag and in critical cases it can cause intake-buzz leading to unstart of vehicle. Hence it becomes important to avoid the separation bubble and if it cannot be avoided then its prediction is important to quantify its effect.

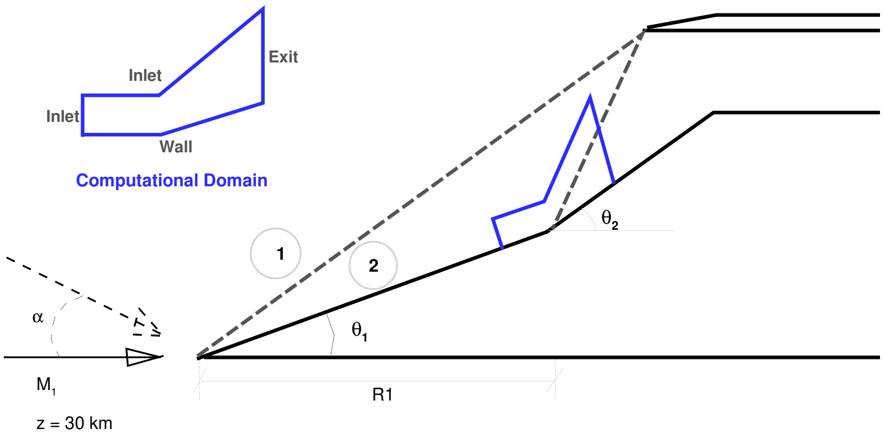

Figure 1: Schematic of scramjet with the computational domain.

Extensive research has been carried out in past, both experimental and computational, in order to understand the physics of flow separation associated with shock-wave interacting with boundary layer for both laminar and turbulent flows across compression corner. Settles et al,[1] Marini et al[2] and Elfstrom[3] found that for higher deflection angle the size of separation bubble increases due to adverse pressure gradient. Ciani et al[4] from their experimental study and Marini et al[2] and Nagaraj et al[5] from their computational study found that as the wall-temperature increases the size of the separation length increases. Elfstrom[3] and Babinsky et al[6] showed that as the Mach number increases the size of separation bubble decreases. With respect to Reynolds number based on boundary layer

*Graduate Student, Department of Aerospace Engineering, Indian Institute of Technology Bombay
†Professor, Department of Aerospace Engineering, Indian Institute of Technology Bombay

thickness Re_δ, Kuehn[7] and Settles et al[8,9] found that as Re_δ increases the size of separation bubble, normalized by the incoming boundary layer thickness, decreases.

In this paper, the various parameters affecting flow-separation in scramjet is studied in detail. The purpose is to understand how the separation bubble behaves with respect to various parameters that frequently vary in flight conditions like the free-stream/flight Mach number, wall-temperature, angle of attack, altitude etc. Understanding these parameters is not a straight forward thing as changes in one parameter leads to simultaneous changes in multiple parameters and it becomes difficult to conclude which parameter exactly has what effect. For this, a canonical case of compression corner, shown in figure-1 as part of scramjet, is considered as a model problem as this allows us to do a controlled study where only canonical parameter can be varied such that all other parameters remain constant. The conditions at station-2 are used as inlet conditions for the simulations. The conclusion drawn from the study of these canonical cases (ramp angle, wall-temperature, Mach number and Reynolds number) would be helpful to understand/justify how the separation bubble would behave when practical parameters of intakes are varied. Further the effect of separation bubble on Lift and Drag of scramjet intake is discussed.

II. Methodology

The standard turbulence models (k-ϵ and k-ω) predicts delayed flow-separation[10,11] and the application of shock-unsteadiness correction[12] moves the separation point closer to the experiments thereby providing better predictions for flow over both compression corner[10] and shock-impingement[13] geometry. However, for lower deflection angles, the effect of the correction term diminishes and thus it does not alter the separation predictions for weakly interacting flows where the standard models give reasonably good predictions. In this work, Favre-averaged Navier-stokes equations[14] are solved for mean flow and shock-unsteadiness modified k-ϵ turbulence model[12] is used for turbulence closure. The computations are done using in-house code well validated and used in various applications[10,15,.16] The governing equations are discretized in finite volume formulation wherein the convective fluxes are solved using low-dissipation modified Steger-Warming flux-splitting method.[17] The viscous fluxes and the turbulent source terms are solved using second order central difference method. The implicit DPLR method[18] is used to integrate in time to achieve steady-state solution. Inlet profiles for the computations are obtained from separate simulations of first ramp wherein the free-stream conditions are applied to inlet and the initial condition for turbulent variables k and ϵ are computed using relations given in reference[19] . No-slip and zero normal pressure gradient is applied to wall and extrapolation boundary conditions are applied to exit plane. Based on grid-convergence study, the computational domain is divided into 200 grid points in wall-normal direction and 170 grid points in stream-wise direction taking the height of domain at start as 0.04m and length as 0.2m + 0.5m which correspond to first and second ramp length respectively. A structured cartesian grid with exponential stretching in y-direction and in x-direction at the corner between the two ramps is used. The Mach number, density and temperature at the design point are M_1 = 6, ρ_1 = 0.01802 kg/m^3 and T_1 = 256.56 K which correspond to an altitude of 30km.

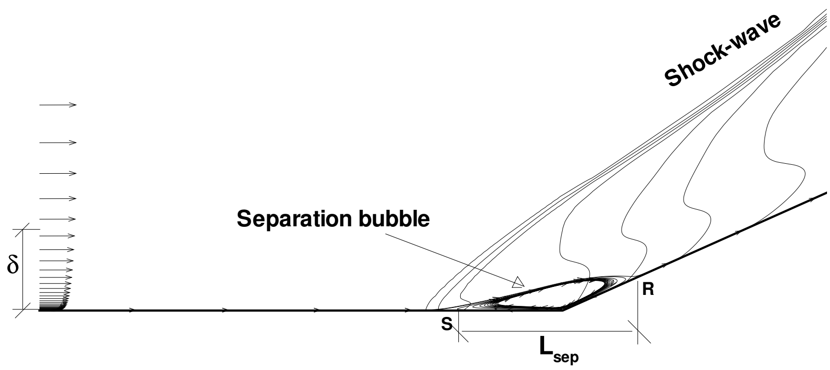

Figure 2: Schematic showing the separation bubble, incoming boundary layer thickness δ and the shock-wave in the computational domain.

At the junction between the two ramps (see schematic in figure-1), the flow would get separated inside the boundary layer leading to formation of separation bubble. Schematic in figure-2 shows the separation bubble length (L_{sep}) and the incoming boundary layer thickness (δ) in the computational domain. In the first part of the study, variation of separation length (L_{sep}/δ) with respect to various canonical parameters is discussed. In the second part of study, variation of separation bubble with respect to various practical parameters is studied and the percentage difference between the analytical and CFD values for Lift and Drag acting on two ramps R1 and R2 is discussed. The total analytical Force acting on two ramps is given as

$$F_{analy} = P_1 R_1 + P_2 R_2 \tag{1}$$

where R_1 and R_2 are length of first and second ramp while P_1 and P_2 are pressure acting on first and second ramp respectively. The total computed force acting on the two ramps is given as

$$F_{CFD} = \sum_{1}^{n} dx_i p_i \tag{2}$$

where p_i is pressure acting at given cell i and dx_i is the distance over which the pressure p_i acts. In order to compute the Lift and Drag due to the above forces, the components of Force are taken in horizontal direction (Drag force F_x) and in vertical direction (Lift force F_y) as given below.

$$F_y = \sum_{1}^{n} p_i dx_i cos\theta_i \tag{3}$$

$$F_x = \sum_{1}^{n} p_i dx_i sin\theta_i \tag{4}$$

where θ_i is ramp angle at a given location which is constant for a given ramp. The Lift and Drag components of analytical forces are calculated using the same equations as above by taking the the horizontal and vertical components of the analytical force given in equation-(1).

III. Results and observations

A parametric study is carried out for high-speed turbulent flow over a compression ramp in order to study the various factors that affect the flow-separation by varying the canonical parameters, discussed in section-A, and practical parameter, discussed in section-B.

A. Effect of canonical parameters

In this section, the variation of separation length normalized by incoming boundary layer thickness with respect to various canonical parameters is discussed in detail.

1. Effect of Ramp angle

Table-1 shows the conditions with which the simulations are done to study the effect of ramp angle. Keeping all conditions constant only the ramp angle θ_2 is varied from 5 to 25° and the results are discussed below.

Table 1: Conditions to be used in simulations to study effect of ramp angle.

M_2	$\theta_2(°)$	$\rho_2(kg/m^3)$	$T_2(°K)$
4.09700	Varying	0.0538	426.5532

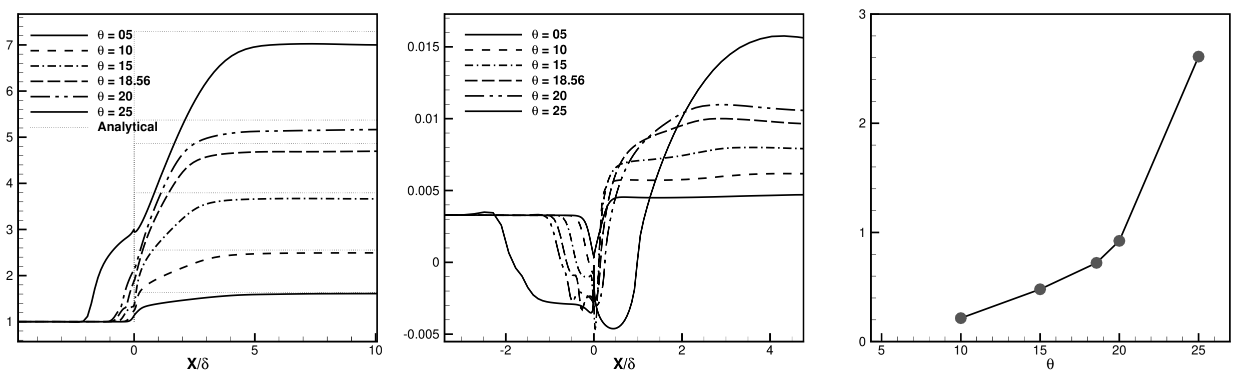

(a) P/P_∞ (b) C_f (c) L_{sep}/δ

Figure 3: (a) Wall-pressure distribution, (b) skin-friction distribution and (c) separation length variation for different ramp angles.

Figure-3 shows the wall-pressure distribution, skin-friction distribution and variation of normalized separation length for different ramp angles. The shock is located at $x/\delta = 0$; left to it correspond to first ramp and right to it correspond to second ramp. Figure-3:a shows the variation of wall-pressure for different ramp angles and is compared with respective analytical solution. It is observed that as ramp angle increases, the pressure jump across shock increases and the upstream influence also increases. The computed pressure profile deviates from the analytical solution near the corner due to the presence of separation bubble. Further the computed pressure is always lower than the analytical ones downstream of shock. Figure-3:b shows the variation of skin-friction over the wall for different ramp angles. The x-location where it takes zero value indicates the separation point 'S' and start of flow-reversal. While the location where it comes back again to zero from negative values indicates the re-attachment point 'R' and the flow in between is reversed. It is observed that as the ramp angle increases, the size of the separation bubble, which is the distance between the separation and re-attachment point, increases. From figure-3:c shows the size of the separation length normalized by the incoming boundary layer thickness (see figure-2) for different ramp angles. As the ramp angle increases, the pressure jump across the shock increases which leads to adverse pressure gradient and hence the flow separates increasing the size of separation bubble.

2. *Effect of wall temperature*

Table-2 shows the conditions with which the simulations are done to study the effect of wall-temperature. Keeping all conditions constant only the wall-temperature is varied from 200 to 600° K and the results are discussed below.

Table 2: Conditions to be used for simulations to study effect of wall-temperature.

M_2	$\theta_2(^\circ)$	$\rho_2(kg/m^3)$	$T_2(^\circ K)$	$T_w(^\circ K)$
4.09700	18.56	0.0538	426.5532	Varying

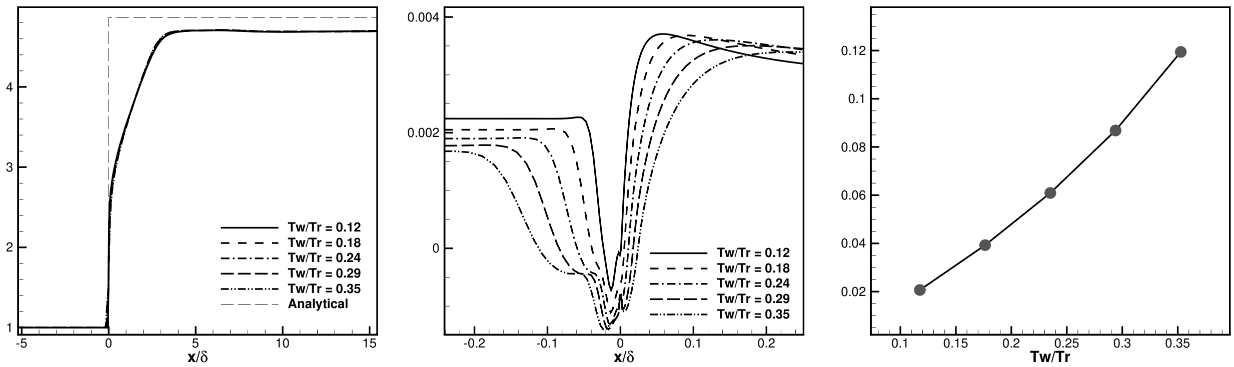

(a) P/P_∞ (b) C_f (c) L_{sep}/δ

Figure 4: (a) Wall-pressure distribution, (b) skin-friction distribution and (c) separation length variation for different wall-temperatures.

Figure-4 shows the wall-pressure distribution, skin-friction distribution and variation of normalized separation length for different wall-temperatures. Figure-4:a shows the variation of wall-pressure for different wall-temperatures and is compared with analytical solution. Since the wall-temperature does not affect the shock-strength, the pressure jump remains same. Figure-4:b shows the skin-friction distribution for different wall-temperatures. It is observed that as the wall-temperature increases, the separation and re-attachment point move away from each other and the separation length increases. Figure-4:c shows the size of the separation bubble normalized by the incoming boundary layer thickness (see figure-2) for different wall-temperatures. As the wall-temperature increases, the near-wall viscosity increases and density decreases. This leads to increase in boundary layer thickness δ and decrease in the skin-friction leading to increase in the size of separation bubble.

3. *Effect of Mach number*

Table-3 shows the conditions with which the simulations are done to study the effect of Mach number. Keeping all conditions constant only the Mach number is varied from 3.0 to 5.0 and the results are discussed below.

Table 3: Conditions to be used for simulations to study effect of Mach numbers.

M_2	$\theta_2(^\circ)$	$\rho_2(kg/m^3)$	$T_2(^\circ K)$	$T_w(^\circ K)$
Varying	18.56	0.0538	426.5532	850

Figure-5 shows the wall-pressure distribution, skin-friction distribution and variation of normalized separation length for different Mach numbers. Figure-5:a shows the variation of wall-pressure for different Mach number

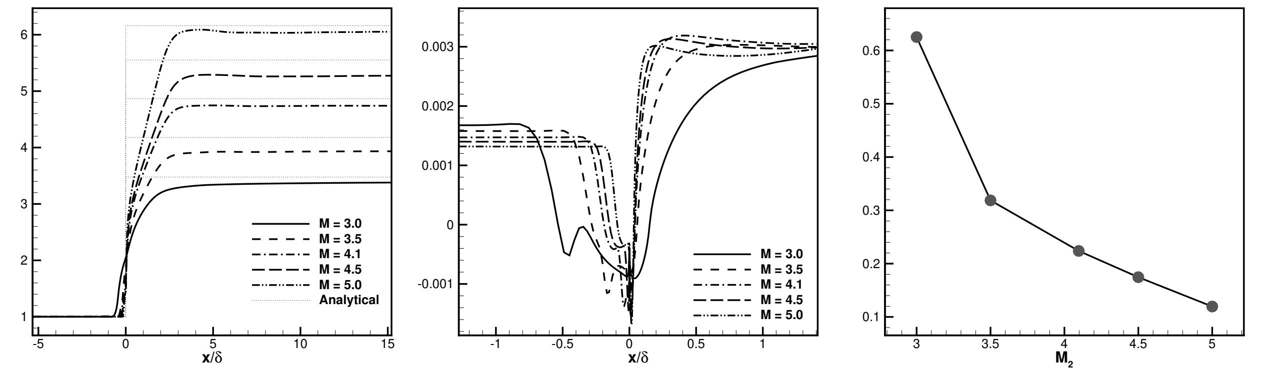

(a) P/P_∞ (b) C_f (c) L_{sep}/δ

Figure 5: (a) Wall-pressure distribution, (b) skin-friction distribution and (c) separation length variation for different Mach numbers.

and is compared with respective analytical solution. As Mach number increases, the pressure jump increases and the upstream influence decreases. Figure-5:b shows the skin-friction distribution for different Mach numbers. It is observed that as the Mach number increases, the size of the separation bubble decreases. Figure-5:c shows the size of the separation length normalized by the incoming boundary layer thickness (see figure-2) for different Mach numbers. As the Mach number increases, even though there is pressure jump, the flow-velocity increases with increasing Mach number and hence the size of the separation bubble decreases.

4. *Effect of Reynolds number*

Table-4 shows the conditions with which the simulations are done to study the effect of Reynolds number. Keeping all conditions constant only the Reynolds number Re_δ is varied from 6.0012e+04 to 1.1327e+05 and the results are discussed below.

Table 4: Conditions to be used for ramp simulations to study effect of Reynolds numbers.

M_2	$\theta_2(^\circ)$	$\rho_2(kg/m^3)$	$T_2(^\circ K)$	$T_w(^\circ K)$	Re_δ
4.09700	18.56	0.05385	426.5532	1300	Varying

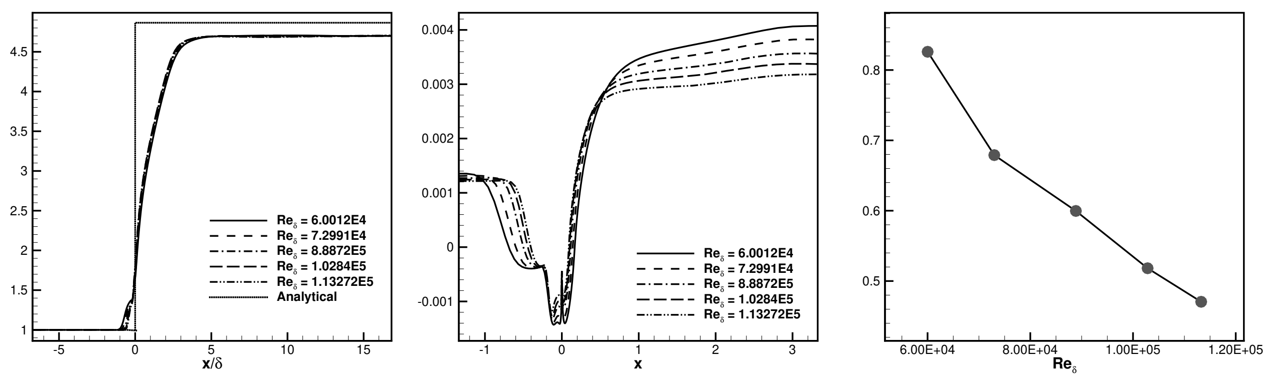

(a) P/P_∞ (b) C_f (c) L_{sep}/δ

Figure 6: (a) Wall-pressure distribution, (b) skin-friction distribution and (c) separation length variation for different Reynolds number Re_δ.

Figure-6 shows the wall-pressure distribution, skin-friction distribution and variation of normalized separation length for different Reynolds number Re_δ . Figure-6:a shows the variation of wall-pressure for different Reynolds numbers and is compared with analytical solution. Changes in Reynolds number does not affect the shock strength, hence the pressure jump remains same for all the cases. Figure-6:b shows the variation of skin-friction for different Reynolds numbers. It is observed that as the Reynolds number increases, the normalized separation length decreases. Figure-6:c shows the size of the separation length normalized by the incoming boundary layer thickness (see figure-2) for different Reynolds numbers. As the Reynolds number Re_δ increases, the flow becomes more turbulent leading to higher increase in boundary layer thickness δ compare to changes in separation length and the normalized separation length decreases.

B. Effect of practical parameters

In this section, the variation of separation length, normalized by incoming boundary layer thickness, with respect to various practical parameters which are always affected by more than one canonical parameters are discussed in detail. The condtions at station-2 are used as the initial condition for all compuations as in section-A. At off-design conditions, for parameter other than being varied, the on-design condition values are used in simulations.

1. Effect of Altitude

As altitude increases, the flow-properties (p,ρ and T) changes as shown in Table-5. Simulations are done by changing altitude given in Table-5 and the results discussed below show the cumulative effect of variation in flow-properties - pressure, temperature and density. Other parameters like wall-temperature, ramp length etc are kept constant.

Table 5: Changes in flow properties (pressure, temperature, density) with change in altitude in atmosphere.

Z (km)	$P_1(Pa)$	$\rho_1(kg/m^3)$	$T_1(^\circ K)$
26	2.1880E+3	3.4260E-2	222.50
28	1.6160E+3	2.5080E-2	224.50
30	1.1719E+3	1.8020E-2	226.65
32	8.8900E+2	1.3550E-2	228.50
34	6.6340E+2	9.8870E-3	233.70

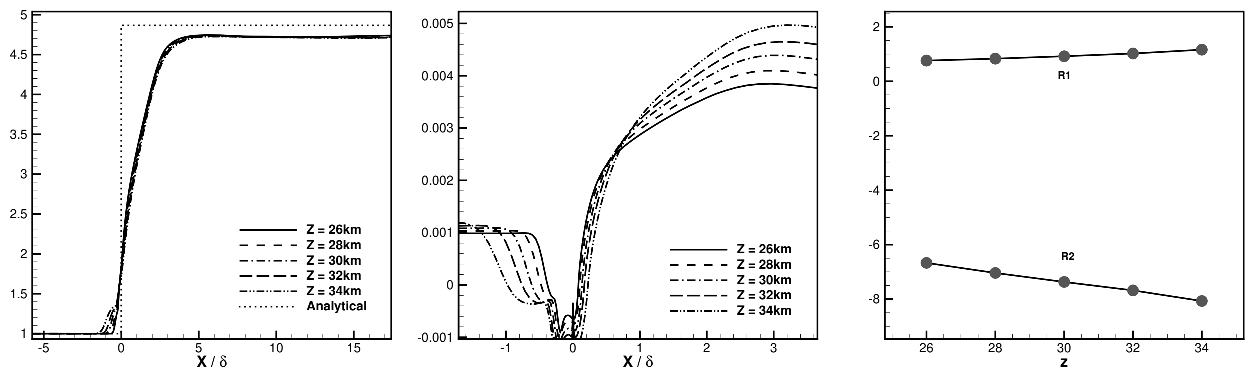

(a) P/P_∞ (b) C_f (c) % change

Figure 7: (a) Wall-pressure distribution, (b) skin-friction distribution and (c) percentage difference between analytical and CFD values of Lift and Drag acting on two ramps for different altitudes.

Figure-7:a shows the distribution of wall-pressure at different altitudes and is compared with analytical solution. As altitude changes, only the flow-properties changes which does not affect the shock strength and hence the pressure jump remains same for all cases. Figure-7:b shows the variation of skin-friction for different altitudes. As the altitude increases, the separation and re-attachment move away from each other increasing the size of the separation length. Figure-7:c shows graphical representation of the percentage difference between the analytical values and the computed values for Lift and Drag forces acting on the first ramp R1 and second ramp R2 at different altitudes. It is seen that the percentage difference is much higher over the second ramp as compare to that over the first ramp. *Note that the actual values of Lift and Drag are much different but the percentage difference with the analytical value remains same.*

2. Effect of flight Mach number

As flight Mach number increases, the flow-properties (p,ρ and T) and Mach number M_2 at station-2 changes as shown in Table-6. Simulations are done by changing flight Mach number M_1 and thus results discussed below show the cumulative effect of changes in Mach number (or shock-strength) and flow-properties (pressure, temperature, density). Figure-9:a shows the distribution of wall-pressure for different flight Mach number and is compared

Table 6: Changes in relevant paramters with change in flight Mach number.

M_1	$\rho_1(kg/m^3)$	$T_1(^\circ K)$	$\theta_1(^\circ)$	M_2	$\rho_2(kg/m^3)$	$T_2(^\circ K)$
4	0.018	256.56	14.18	2.99	0.0416	341.74
5	0.018	256.56	14.18	3.58	0.0478	380.91
6	0.018	256.56	14.18	4.10	0.0538	426.55
7	0.018	256.56	14.18	4.53	0.0595	478.93
8	0.018	256.56	14.18	4.90	0.0647	538.31

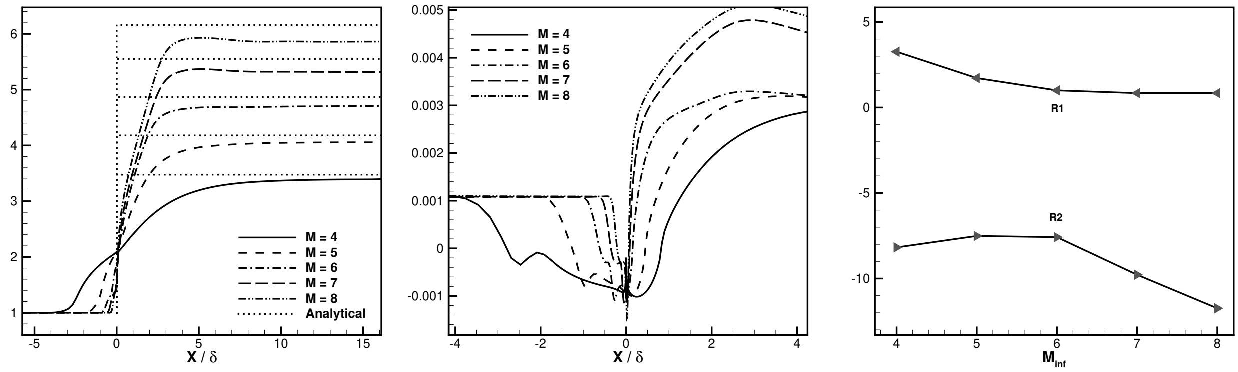

(a) P/P_∞ (b) C_f (c) % change

Figure 8: (a) Wall-pressure distribution, (b) skin-friction distribution and (c) percentage difference between analytical and CFD values of Lift and Drag acting on two ramps for different flight Mach numbers.

with respective analytical solution. As Mach number increases, the pressure jump increases. Figure-9:b shows the variation of skin-friction for different flight Mach numbers. It is observed that as the flight Mach number increases, the separation and re-attachment point move closer to each other and the size of the separation bubble decreases. Figure-9:c shows graphical representation of the percentage difference between the analytical values and the computed values for Lift and Drag forces acting on the first ramp R1 and second ramp R2 for different flight Mach numbers. It is seen that over the first ramp the percentage difference is within 5% whereas over the second ramp it can be as high as 12% for higher off-design conditions.

3. Effect of Ramp length

As the first ramp length is increased, keeping the shock-on-lip condition satisfied, the second ramp angle θ_2 and Reynolds number Re_δ both gets changed and all other relevant parameters remains same as shown in Table-7. Simulations are done by changing first ramp length R1 using conditions given in Table-7 and the results discussed below show the cumulative effect of changes in ramp angle θ_2 and Reynolds number Re_δ. Figure-9:a shows the distribution of wall-pressure for different first ramp length R1 and is compared with respective analytical solution. As ramp length increases, the pressure jump increases due to increase in second ramp angle to satisfy the shock-on-lip condition and the upstream influence increases. Figure-9:b shows the distribution of skin-friction for different lengths of first ramp. It is observed that as the first ramp length increases, the separation and re-attachment points move away from each other and the normalized separation length increases. Figure-9:c shows

Table 7: Variation of relevant parameters for different first ramp length R1.

M_1	$R1(m)$	$\theta_2(^\circ)$	M_2	Re_δ	$\rho_2(kg/m^3)$	$T_2(^\circ K)$
6	1.50	4.99	4.10	9.1239e+04	0.05385	426.55
6	1.75	10.33	4.10	1.0090e+05	0.05385	426.55
6	2.00	18.56	4.10	1.1678e+05	0.05385	426.55
6	2.25	30.63	4.10	1.2842e+05	0.05385	426.55

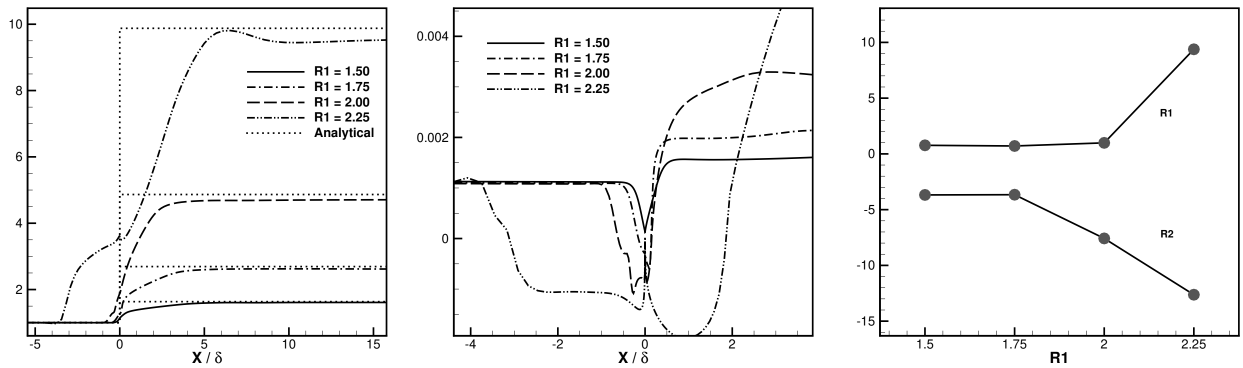

(a) P/P_∞ (b) C_f (c) % change

Figure 9: (a) Wall-pressure distribution, (b) skin-friction distribution and (c) percentage difference between analytical and CFD values of Lift and Drag acting on two ramps for different lengths of first ramp R1.

graphical representation of the percentage difference between the analytical and the computed values for Lift and Drag forces acting on the first ramp R1 and second ramp R2 for different lengths of first ramp R1. For smaller length of first ramp, the percentage difference is very small but becomes quite high for higher ramp lengths and the percentage difference over the second ramp is comparatively much higher compare to that at first ramp.

4. *Effect of angle of attack*

As the angle of attack α changes, the apparent first ramp angle $\theta_1^\star$ changes (though physically the first ramp angle remains same, since flow angle at inlet is changing the apparent first ramp angle changes and is given as $\theta_1^\star = \theta + \alpha$). Due to the change in apparent first ramp angle, the Mach number M_1 at station-1 also gets varied. Thus changes

Table 8: Variation of relevant parameters for different angles of attack.

M_1	$\theta_1(^\circ)$	$\alpha(^\circ)$	$\theta_1^\star(^\circ)$	M_2	$\rho_2(kg/m^3)$	$T_2(^\circ K)$
6	14.18	+4	18.18	3.5962	6.3047E-2	5.1797E+2
6	14.18	+2	16.18	3.8425	5.8635E-2	4.6996E+2
6	14.18	0	14.18	4.0970	5.3841E-2	4.2635E+2
6	14.18	-2	12.18	4.3583	4.8716E-2	3.8711E+2
6	14.18	-4	10.18	4.6237	4.3349E-2	3.5212E+2

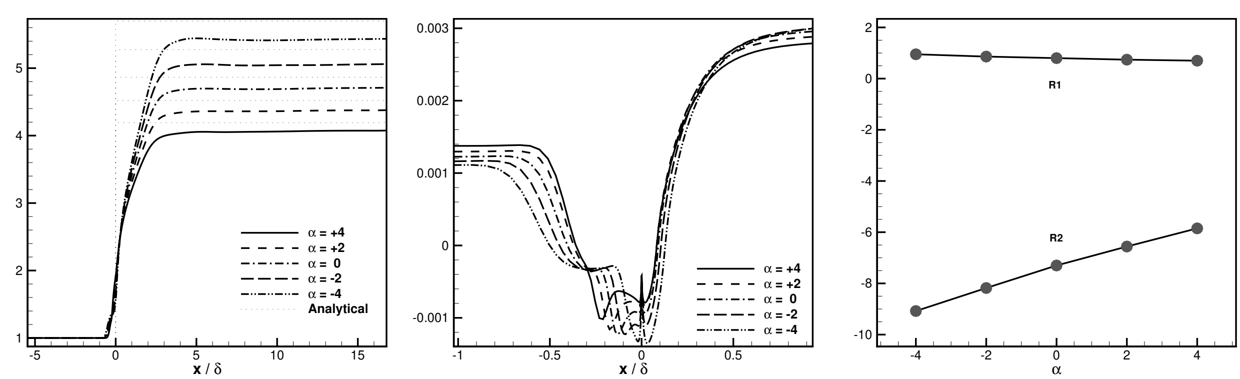

(a) P/P_∞ (b) C_f (c) % change

Figure 10: (a) Wall-pressure distribution, (b) skin-friction distribution and (c) percentage difference between analytical and CFD values of Lift and Drag acting on two ramps for different angles of attack.

in angle of attack is cumulative effect of changes in ramp angle and Mach number and the results are as discussed below. Simulations are done for different angles of attack using conditions given in Table-8 and results discussed below show the cumulative effect of changes in ramp angle θ_2 and Reynolds number Re_δ. Figure-10:a shows the distribution of wall-pressure at different angles of attack. As the angle of attack increases, the pressure jump decreases due to decrease in Mach number. Figure-10:b shows the distribution of skin-friction for different angles of attack. It is observed that as the angles of attack increases, the size of the separation bubble decreases.Figure-10:c shows graphical representation of the percentage difference between the analytical values and the computed values for Lift and Drag forces acting on the first ramp R1 and second ramp R2 for different angles of attack. Similar to previous cases, the percentage difference over the second ramp is much higher compare to that over the first ramp.

IV. Summary and conclusions

In first part of the study, how separation bubble gets affected by various canonical parameters is discussed while in the second part the percentage difference between the analyitical and computed values of Lift and Drag forces acting on the two ramps is discussed along with the changes in the separation length. From the study of canonical parameters it is observed that the separation length normalized by the incoming boundary layer thickness increases with (i) increase in ramp angle (ii) increase in wall-temperature (iii) decrease in Mach number and (iv) increase in Reynolds number Re_δ as shown in Table-9. From the study of practical parameters it is observed that the separation length normalized by the incoming boundary layer thickness increases with (i) increase in altitude (ii) decrease in flight Mach number (iii) increase in Ramp length and (iv) increase in Reynolds number Re_δ as shown in Table-10.

Table 9: Variation of normalized separation length with respect to various canonical parameters.

Canonical parameters	Separation length
$\theta \uparrow$	$L_{sep}/\delta \uparrow$
$M \uparrow$	$L_{sep}/\delta \downarrow$
$Re_\delta \uparrow$	$L_{sep}/\delta \downarrow$
$T_w/T_r \uparrow$	$L_{sep}/\delta \uparrow$

Table 10: Variation of normalized separation length with respect to various practical parameters.

Practical parameters	Separation length
z $\uparrow$	$L_{sep}/\delta \uparrow$
$M_\infty \uparrow$	$L_{sep}/\delta \downarrow$
$R1 \uparrow$	$L_{sep}/\delta \uparrow$
$\alpha \uparrow$	$L_{sep}/\delta \downarrow$

Presence of separation bubble in intakes is critical as it alters distribution of wall-pressure over the surface leading to changes in the aerodynamic properties. This alteration deteriorates the aerodynamic performance of the vehicle surface. Of all the cases considered in this study, the worst case scenario is for the off-design condition operation at high Mach number of M = 8 wherein the percentage difference can be high up-to 12%. If variation in ramp length is considered (flexible geometry) then the first ramp length of R1 = 2.25m is the worst case scenario wherein the percentage difference can exceed the 12% range. This high percentage difference occurs over the second ramp where the effect of both separation bubble and the separation shock is seen due which the computed results deviate from the analytical data by large margin.

References

[1]Settles, G. S., Fitzpatrick, T. J., and Bogdonoffj, S. M., "Detailed Study of Attached and Separated Compression Corner Flowfields in High Reynolds Number Supersonic Flow," *AIAA Paper*, Vol. 17, No. 6, 1979.

[2]Marini, M., "Effects of flow and geometry parameters on shock-wave boundary-layer interaction phenomena," *8th AIAA International Space Planes and Hypersonic Systems and Technologies Conference*, 1998, pp. 319–329.

[3]Elfstrom, G., "Turbulent hypersonic flow at a wedge-compression corner," *Journal of Fluid Mechanics*, Vol. 53, No. 01, may 1972, pp. 113.

[4]Ciani, A., Paris, S., and Fletcher, D. G., "Studies of wall temperature effects on shock- wave / boundary layer interactions in hypersonic flow," *6th International conference on quantitative infrared thermography QIRT 2002*, No. September 24-27, 2002, pp. 120–125.

[5]Nagaraj, B. and Zakiuddin, M., "Effect of Reynolds Number and Wall Temperature on Shock Wave / Boundary Layer Interaction," *International Journal & Magazine of Engineering, Technology, Management And Research*, Vol. 3, No. 10, 2016, pp. 527–539.

[6]Babinsky, H. and Harvey, J. K., *Shock Wave Boundary Layer Interactions*, Cambridge University Press, Cambridge, 2011.

[7]Kuehn, D. M., "Experimental Investigation of the Pressure Rise Required for the Incipient Separation of Turbulent Boundary Layers in Two-Dimensional Supersonic Flow," Tech. Rep. February 1959, 1959.

[8]Settles, G. S., Bogdonoff, S. M., and Vas, I. E., "Incipient Separation of a Supersonic Turbulent Boundary Layer at High Reynolds Numbers," *AIAA Journal*, Vol. 14, No. 1, 1976, pp. 50–56.

[9]Settles, G. S. and Bogdonofft, S. M., "Scaling of Two-and Three-Dimensional Shock/Turbulent Boundary-Layer Interactions at Compression Corners," *AIAA JOURNAL*, Vol. 20, No. 6, 1982.

[10]Sinha, K., Mahesh, K., and Candler, G. V., "Modeling the Effect of Shock Unsteadiness in Shock/ Turbulent Boundary-Layer Interactions," *AIAA Journal*, Vol. 43, No. 3, mar 2005, pp. 586–594.

[11]Oliver, A. B., Lillard, R. P., Schwing, A. M., Blaisdell, G. A., and Lyrintzis, A. S., "Assessment of Turbulent Shock-Boundary Layer Interaction Computations Using the OVERFLOW Code," *45th AIAA Aerospace Sciences Meeting and Exhibit*, No. January, American Institute of Aeronautics and Astronautics, Reston, Virigina, jan 2007, pp. 8–11.

[12]Sinha, K., Mahesh, K., and Candler, G. V., "Modeling shock unsteadiness in shock/turbulence interaction," *Physics of Fluids*, Vol. 15, No. 8, 2003, pp. 2290.

[13]Ali Pasha, A. and Sinha, K., "Shock-unsteadiness model applied to oblique shock wave/turbulent boundary-layer interaction," *International Journal of Computational Fluid Dynamics*, Vol. 22, No. 8, sep 2008, pp. 569–582.

[14]Wilcox, D. C., *Turbulence modeling for CFD*, 1998.

[15]Sinha, K., "Shock / turbulence interaction : turbulence modeling and scramjet application," *11th CFD Symposium*, , No. August, 2009, pp. 1–8.

[16]Sinha, K., Rane, N. J., and Pawar, V., "Numerical investigation of three-dimensional shock / boundary-layer interaction in a hypersonic inlet," *28th Shock Waves Symposium*, 2011, pp. 1–6.

[17]Steger, J. L. and Warming, R. F., "Flux vector splitting of the inviscid gasdynamic equations with application to finite-difference methods," *Journal of Computational Physics*, Vol. 40, No. 2, apr 1981, pp. 263–293.

[18]Wright, M. J., *A family of data-parallel relaxation methods for the Navier-Stokes equations*, Ph.D. thesis, UNIVERSITY OF MINNESOTA, 1997.

[19]Menter, F. R., "Two-equation eddy-viscosity turbulence models for engineering applications," *AIAA Journal*, Vol. 32, No. 8, 1994, pp. 1598–1605.